Theoretical and Applied Climatology (2020) 142:349–367
https://doi.org/10.1007/s00704-020-03283-4

ORIGINAL PAPER

A novel approach for predicting daily pan evaporation in the coastal regions of Iran using support vector regression coupled with krill herd algorithm model

Yiqing Guan[1] · Babak Mohammadi[1] · Quoc Bao Pham[2,3] · S. Adarsh[4] · Khaled S. Balkhair[5] · Khalil Ur Rahman[6] · Nguyen Thi Thuy Linh[7] · Doan Quang Tri[8]

Received: 1 January 2020 / Accepted: 1 June 2020 / Published online: 13 July 2020

Abstract

Evaporation is one of the vital components of hydrological cycle. Precise estimation of pan evaporation (E_{pan}) is essential for the sustainable water resources management. The current study proposed a novel approach to estimate daily E_{pan} across the humid region of Iran using support vector regression (SVR) technique coupled with Krill Herd Algorithm (SVR-KHA). Meteorological data were collected from three stations (Bandar Abbas, Rudsar, and Osku) over a period from 2008 to 2018 and used for application. Of the data, 70% were used for training and remaining 30% were used for testing. The study considered seven different combinations of input variables for predicting daily E_{pan} at each station. The influence of KHA hybridization is examined by comparing results of SVR-KHA algorithm with simple SVR through a multitude of statistical performance evaluation criteria such as coefficient of determination (R^2), Wilmot's index (WI), root-mean-square error (RMSE), Mean Absolute Error (MAE), Relative Root Mean Square Error (RRMSE), Mean Absolute Relative Error (MARE), and several graphical tools. Single input SVR1 model hybrid with KHA (SVR-KHA1) showed improved performance (R^2 of 0.717 and RMSE of 1.032 mm/day) as compared with multi-input SVR models, e.g., SVR5 (with RMSE and MAE of 1.037 mm/day and 0.773 mm/day), while SVR7 model hybridized with KHA (SVR-KHA7), which considers seven meteorological variables as input, performed best as compared with other models considered in this study. E_{pan} estimates at Bandar Abbas and Rudsar by SVR and SVR-KHA are similar (with R^2 statistics values of 0.82 and 0.84 at Bandar Abbas station, and 0.88 and 0.9 at Rudsar station, respectively). However, better improvements in E_{pan} estimates are observed at Osku station (with R^2 of 0.91 and 0.86, respectively), which is situated at interior geographical location with a higher altitude than the other two coastal stations. Overall, the results showed consistent performance of SVR-KHA model with stable residuals of lower magnitude as compared with standalone SVR models.

1 Introduction

Evaporation accounts for water losses from the land surface and water bodies. It is, therefore, a critical component of the hydrological cycle which plays a key role in water resources management, agricultural production, hydrological modeling, design of irrigation systems, and irrigation scheduling (Moazenzadeh et al. 2018; Gundalia and Dholakia 2013;

✉ Doan Quang Tri
doanquangtri@tdtu.edu.vn

[1] College of Hydrology and Water Resources, Hohai University, Nanjing 210098, China

[2] Institute of Research and Development, Duy Tan University, Danang 550000, Vietnam

[3] Faculty of Environmental and Chemical Engineering, Duy Tan University, Danang 550000, Vietnam

[4] Department of Civil Engineering, TKM College of Engineering Kollam-691005, Kollam, India

[5] Department of Hydrology and Water Resources Management, Faculty of Meteorology, Environment and Arid Land Agriculture, King Abdulaziz University, Jeddah, Saudi Arabia

[6] State Key Laboratory of Hydroscience and Engineering, Department of Hydraulic Engineering, Tsinghua University, Beijing, China

[7] Thuyloi University, 175 Tay Son, Dong Da, Hanoi, Vietnam

[8] Sustainable Management of Natural Resources and Environment Research Group, Faculty of Environment and Labour Safety, Ton Duc Thang University, Ho Chi Minh City, Vietnam

Fan et al. 2016; Feng et al. 2018). The evaporation process is stimulated by several atmospheric and climate variables such as temperature, rainfall, humidity, solar radiation, wind, and drought dispersion. It is always considered an atmospheric evaporative demand indicator under a climate change scenario (Roderick et al. 2014). The most influential factors for evaporation are vapor pressure gradient and heat energy, which largely depend on atmospheric variables (Vicente-Serrano et al. 2018; Fan et al. 2018a, b). These factors are further dependent on time of the day, geographical location, and climate and seasonal variations (Lu et al. 2018). Evaporation, calculation wise, is highly nonlinear; it is very difficult to estimate through climatic factors especially in variable climate conditions.

Precise assessment of pan evaporation (E_{pan}) is of paramount importance for sustainable water resources management (Feng et al. 2018). Class A Pan evaporation and Eddy correlation system methods are the standard techniques for direct estimation of E_{pan}. However, high cost and maintenance, suboptimal instrumental, and practical issue constraints the direct measurement of E_{pan} both on spatial and temporal scales (Ding et al. 2011; Shiri et al. 2014). Therefore, several alternative techniques, such as empirical Stephens and Stewart (SS) model, physically-based PenPan model, mass transfer-based models, temperature-based models, solar radiation-based models, data-driven models, etc., are developed for indirect estimation of E_{pan} from atmospheric variables (Kim and Kim 2008; Xu and Singh 1998, 2000, 2001; Singh and Xu 2015). Yang and Yang (2012) modified Class A pan model and developed PenPan model to estimate the Chinese D20 pan evaporation and quantify contributions of climate factors at 54 meteorological stations across China. PenPan model was used to assess global climate models' performances in projecting monthly, seasonal, and annual statistics of E_{pan} across China (Liu and Sun 2016). Singh and Xu (2015) evaluated the dependence of different mass transfer-based evaporation models on various meteorological variables over different time scales. Donohue et al. (2010) estimated E_{pan} across Australia by comparing five potential evaporation formulations and found that four-variable Penman formulation performed well to estimate potential evaporation dynamics. Similarly, Gundalia and Dholakia (2013) predicted daily E_{pan} based on solar radiation and air temperature using six empirical models. They found that radiation-based Jensen model is more reliable to estimate E_{pan} in Junagadh, India. Most recently, Feng et al. (2018) assessed the performance of the PenPan model and SS model (radiation-based) to estimate E_{pan} over different climate regions of China. They reported better performance of the SS model when only global air temperature and solar radiation data are available across temperate continental zones and mountain plateau.

The estimation of E_{pan} is very complex and extremely nonlinear. Due to complexities and deficiencies in empirical models, data-driven approaches, including machine learning algorithms, are successfully applied because they propose simple solutions for multi-variable non-linear functions and independent of internal variables (Kisi 2015; Wang et al. 2017a, b). Therefore, several machine learning algorithms and models are proposed to estimate E_{pan}, e.g., artificial neural network (ANN) (Kisi 2013; Khoob 2008; Goyal et al. 2014; Dalkili et al. 2014), support vector machines (SVM) (Kim et al. 2012; Lin et al. 2013; Kisi 2015; Wang et al. 2016a, b; Moazenzadeh et al. 2018), adaptive neuro-fuzzy inference system (ANFIS) (Sanikhani et al. 2012; Piri et al. 2012, 2016; Kisi and Tombul 2013; Goyal et al. 2014), generalized regression neural networks (GNN) (Kim and Kim 2008; Kim et al. 2013; Feng et al. 2017), multiple layer perceptron (MLP) (Kisi 2008; Kim et al. 2013; Ghorbani et al. 2018), extreme learning machine (ELM) (Deo et al. 2016; Feng et al. 2018), etc. These data-driven approaches significantly improved the estimation accuracy of E_{pan} in data-scarce regions because these methods deal with the non-linear relationships between the independent and dependent variables exceptionally well.

Evolutionary neural network (ENN) developed by Kisi (2013) for modeling E_{pan} on the monthly scale across the Mediterranean region of Turkey and the performance of ENN was compared with fuzzy genetic (FG), neuro-fuzzy, ANN, and SS models. The results demonstrated a better prediction accuracy of ENN in comparison with other models. Lin et al. (2013) compared SVM and MLP models across Taiwan of China and confirmed high accuracy of the SVM model in estimating E_{pan} due to the robust model, high computational efficiency and accuracy. The performance of MLP and cascade correlational neural networks (CCNN) was assessed in the Republic of Korea by Kim et al. (2014). Results indicated that in the testing stage, the CCNN outperformed MLP model for homogeneous and heterogeneous meteorological stations. Malik and Kumar (2015) evaluated co-active adaptive neuro-fuzzy inference system (CANFIS), ANN, and MLR models across Pantnagar, India. Their study reported better performance of ANN as compared with MLR and CANFIS. Wang et al. (2017a, b) compared MLP, generalized regression neural network (GRNN), FG, multi-variate adaptive regression spline (MARS), and ANFIS with girded partition (ANFIS-GP), and the least square support vector machine (LSSVM) models along with two empirical models for monthly scale E_{pan} estimation in different climate regions of China during 1961–2000. They reported better performance of MLP using local input data at most of the stations, while GRNN outperformed the rest of the models across Tibetan Plateau. Feng et al. (2018) compared the performance of ELM, artificial neural networks optimized by particle swarm optimization (PSO-ANN) and genetic algorithm (GA-ANN) models to estimate PE across different climate regions across China. ELM model performed well when all input data were available, PSO-ANN was recommended for mountain plateau and GA-ANN for temperate monsoon and continental season having only air temperature available.

Furthermore, several optimization algorithms such as ant colony (AC), wolf search algorithm (WSA), whale optimization algorithm (WOA), and firefly algorithm (FA) are successfully used very recently as a novel optimization technique in hydrology (Mohammadi and Aghashariatmadari 2020; Jahani and Mohammadi 2019), reference evapotranspiration modeling (Mohammadi and Mehdizadeh 2020), soil physics variables (Vaheddoost et al. 2020), water resources management (Mohammadi et al. 2020; Pham et al. 2020; Moazenzadeh et al. 2018), and soil science (Moazenzadeh and Mohammadi 2019). SVM, SVM-FA (SVM coupled with FA), and ANN optimization algorithms are used to predict soil moisture content at field capacity (FC) and PWP (permanent welting point). SVM-FA algorithm yielded best estimates (Ghorbani et al. 2017). A coupled grouping genetic-extreme learning machine (GGA-ELM) model was proposed and used to estimate the solar radiation in Spain (Aybar-Ruiz et al. 2016). The SVR-FA (support vector regression coupled with Firefly algorithm) is used for long-term forecasting of monthly average temperature (Kavousi-Fard et al. 2014; Moazenzadeh et al. 2018; Mehr et al. 2019). Jahani and Mohammadi (2019) used ANN and ANN-GA (ANN coupled with genetic algorithm) to estimate daily solar radiation.

Evaporation from water bodies has significantly affected the agricultural regions of Iran and other dry regions. More than 40% of water loss is attributed to E_{pan} (Prime et al. 2012). However, very limited studies have evaluated the data-driven (empirical) models to estimate the E_{pan} across Iran. Tabari et al. (2009) evaluated the performance of ANN and multivariate non-linear regression (MNLR) models to simulate daily E_{pan} in a semi-arid region of Iran. The results revealed that ANN provided the best estimation of daily E_{pan} as compared with MNLR. Kim et al. (2012) evaluated multi-layer perceptron-neural networks (MLP-NN), GRNN, and support vector machine-neural networks (SVM-NN) to estimate daily E_{pan} in various climate regions of Republic of Korea and Iran, and reported better SVM-NN performance. Kim et al. (2015) developed MLP-NNM, Kohonen self-organizing feature maps-neural networks model (KSOFM-NNM), and gene expression programming (GEP) for daily E_{pan} estimation in south-western Iran having dry climate.

To proceed with the development and application of data-driven models, the objective of this study is to propose and apply a novel approach to estimate daily E_{pan} using support vector regression technique coupled with Krill Herd Algorithm (SVR-KHA) across the coastal (humid) region of Iran.

2 Materials and methods

2.1 Study area and datasets used

In this study, evaporation data of the stations Bandar Abbas, Osku, and Rudsar in the coastal regions of Iran were considered for modeling (Fig. 1). The Bandar Abbas station is located in a port city with altitude of 9.8 m on the southern coast of Iran across the Persian Gulf. The Osku station is located in northwestern Iran with altitude of 1428 m. It is near the Lake Urmia, the largest lake in the Middle East. Osku has a humid continental climate characterized with warm to hot (and often humid) summer and cold winter seasons. The annual precipitation is around 320 mm. The Rudsar station is situated in the north of Iran near the Caspian Sea, which is the largest lake of the world, having altitude of − 22 m. Rudsar either has a very humid climate, with warm summer and cool winter seasons. Rudsar station sometimes receives snow during the cool winter season. It has also a relatively continental climate with cold winter and higher seasonal temperature variation than most of Iran.

This study focuses on three coastal regions, which are of utmost importance to Iran. The Bandar Abbas station is an important location for maritime trade and oil transportation in the Middle East countries. The Rudsar station is located in the vicinity of largest lake on the earth (Caspian Sea), while the Osku station is situated near the sixth-largest saltwater lake on the Earth (Lake Urmia) and also the most important lake in the Middle East. Table 1 presents the geographical location of the selected three stations (latitude and longitude), altitude, and data period.

Different variables are considered for estimation of daily E_{pan} (mm) including daily values of maximum temperature (°C), mean wind speed (m/s), mean vapor pressure (kPa), total rainfall (mm), mean relative humidity (%), total sunshine hours (hrs), and solar radiation (MJ m^{-2} day^{-1}). The different meteorological data were collected from the Iran Meteorological Organization (IMO). The time series of daily E_{pan} of the three stations are presented in Fig. 2. A rigorous quality check was performed on the collected database before proceeding with the modeling. It is highly necessary to ensure that the record structure of data is correct and complete before proceeding with modeling of any time series and there are definite procedures to perform the quality control of the datasets (Feng et al. 2004; Estévez et al. 2016). In this study, we identified that only 0.05% of the whole data of Bandar Abbas, Osku, and Rudsar stations are found to be missing or outliers in the 10-year-period chosen for the analysis (Feng et al. 2004). The flagged outlier (incorrect data) was also considered missing, and artificial neural network (ANN) method was invoked to fill this missing information. Finally, the range test was used to ensure that the obtained missing values are within the range of the weather stations operated by IMO (Estévez et al. 2016), the magnitudes are within acceptable range (mean ± standard deviation), and statistical properties of the dataset gets preserved. The statistical properties of the training (70% of total data) and testing (30% of total data) are provided in Table 2.

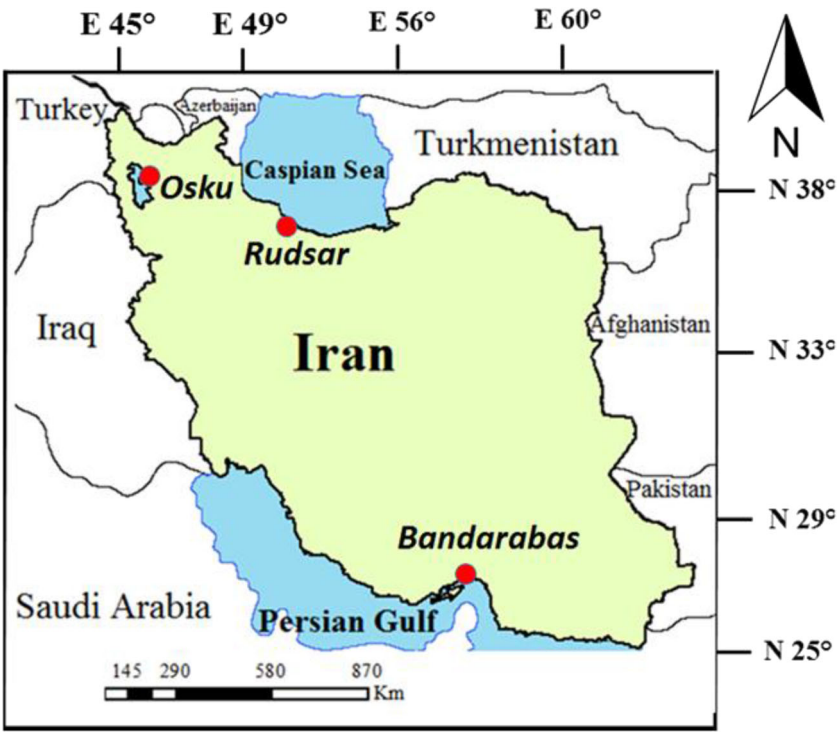

Fig. 1 Location of the study area and selected stations

2.2 Predictor models

In the present study, the collected meteorological data recorded at three meteorological stations is used as inputs of predictor models, and daily E_{pan} is the output of predictor models. The classic SVR and SVR-KHA models are used as predictor models to predict daily E_{pan} in the coastal regions of Iran. Figure 3 shows schematic structure of inputs, output, and modeling process for this study.

2.2.1 Classic support vector regression (SVR)

Support vector regression (SVR), which was introduced by Vapnik and Chervonenkis (1974) based on the theory of statistical learning, is a set of supervised learning methods used for classification and regression tasks. SVR is a popular technique for prediction, pattern recognition, classification, regression, and function approximation (Moazenzadeh et al. 2018; Aghelpour et al. 2019). Vapnik et al. (1997) introduced SVMs for dividing a set of vectors into two classes. SVMs are based on a hyperplane in the form of $w.X+b=0$ that optimally separates a set of n-dimensional vectors ($X_i \in R^n$) into two categories. This optimal hyperplane has the farthest distance from support vectors and the nearest data points from each class. Finding w is equivalent to solving a quadratic programming problem. To solve this problem, a trade-off parameter ($c>0$) needs to be determined. To categorize vectors that are not linearly separable, a kernel function such as degree-d polynomial, radial basis, or hyperbolic tangent is used to map the observed multidimensional vectors to a space with higher dimensions (Moazenzadeh and Mohammadi 2019; Mohammadi 2020). The following radial basis function was used:

$$k(X_i, X_j) = \exp\left(-\gamma \left\| X_i - X_j \right\|^2\right) \quad (1)$$

where $\gamma > 0$ is the parameter of the kernel *and* X_i, X_j represent feature vectors in some input space. The nonlinear regression version of SVMs is written as follows:

$$y = \sum_{i=1}^{m} \left(g_i - g_i^*\right) k(X_i, X_j) + b \quad (2)$$

where m indicates total number of input data; g_i and g_i^* are the Lagrange multipliers for upper and lower

Table 1 Location details of stations and duration of available data

Station name	Duration	Latitude	Longitude	Altitude (m)
Bandar Abbas	2/20/2008–2/18/2018	27°13′ N	56° 22′ E	9.8
Osku	1/1/2009–12/31/2018	37° 9′ N	46° 14′ E	1428
Rudsar	3/20/2008–3/19/2018	37° 70′ N	50° 19′ E	−22

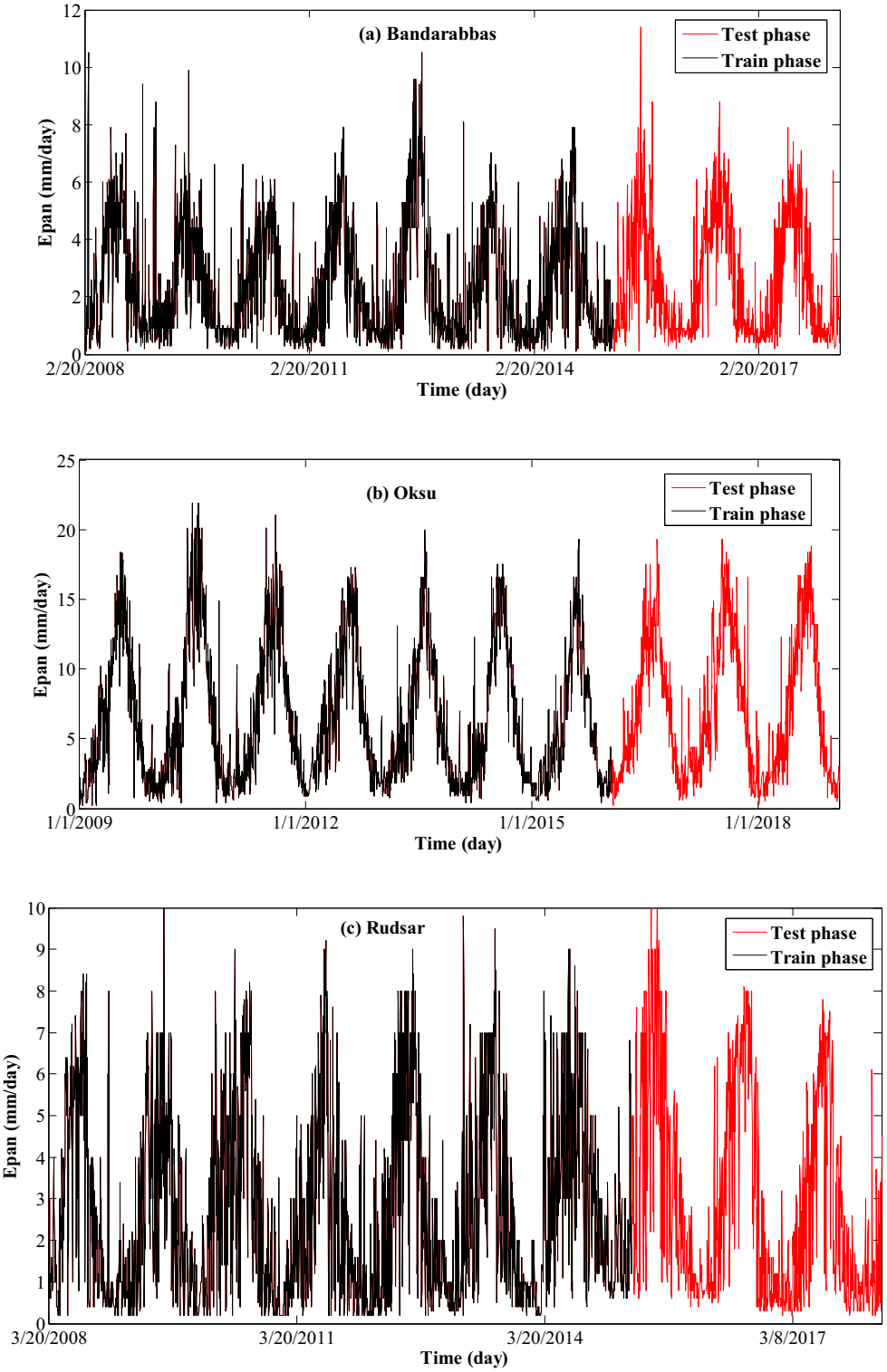

Fig. 2 Variation of daily evaporation time series duration of study periods at three stations (**a**) Bandar Abbas, (**b**) Osku, (**c**) Rudsar

constraints, respectively, and k denotes the kernel function employed to map the n-dimensional input vectors. There are some fundamental kernel functions provided by support vector machines such as linear, polynomial, sigmoid, and radial basis functions. Among these functions, radial basis function (RBF) was used by some researchers (Mohammadi and Mehdizadeh 2020), then RBF kernel selected for this study.

Table 2 Statistical properties of datasets used for pan evaporation (E_{pan}) prediction

Stations	Variables	Training phase					Testing phase				
		X_{min}	X_{max}	X_{mean}	$X_{st.\ dev.}$	X_{cv}	X_{min}	X_{max}	X_{mean}	$X_{st.\ dev.}$	X_{cv}
Bandar Abbas	T_{max} (°C)	− 1.4	38	21.09	8.43	0.39	− 1.2	37.5	21.18	8.36	0.39
	RH_{mean} (%)	16	99	80.67	9.66	0.11	32	100	80.35	9.99	0.12
	P (mm)	0	141.3	3.36	10.33	3.07	0	92.4	3.79	10.88	2.86
	SSH (hr)	0	13.4	4.8	4.16	0.86	0	13	4.95	4.3	0.86
	W (m/s)	0	20	4.27	1.81	0.42	0	18	4.32	1.86	0.43
	e_s-e_a (KPa)	0.01	2.59	0.46	0.36	0.78	0	1.87	0.48	0.39	0.8
	R_S (MJ m^{-2} day^{-1})	1.17	18.22	7.86	4.7	0.59	2.15	18.09	7.99	4.88	0.61
	E_{pan} (mm day^{-1})	0.1	10.5	2.39	1.91	0.8	0.1	11.4	2.51	1.93	0.76
Osku	T_{max} (°C)	− 1.6	44.8	22.86	8.78	0.38	− 1	42	23.45	8.46	0.36
	RH_{mean} (%)	10	95	61.53	11.92	0.19	17	100	62.29	12.28	0.19
	P (mm)	0	34.2	0.61	2.38	3.86	0	37.6	0.64	2.76	4.27
	SSH (hr)	0	13	7.52	3.61	0.48	0	12.8	7.72	3.48	0.45
	W (m/s)	0	33	11.8	5.4	0.45	0	22	10.68	4.94	0.46
	e_s-e_a (KPa)	0.03	3.57	0.98	0.65	0.66	0	4.1	0.99	0.65	0.65
	R_S (MJ m^{-2} day^{-1})	1.55	17.65	8.89	4.89	0.55	1.69	17.89	9.08	4.93	0.54
	E_{pan} (mm day^{-1})	0.2	21.9	8.89	4.89	0.55	0.2	19.3	6.94	4.86	0.7
Rudsar	T_{max} (°C)	0	37.4	21.08	8.28	0.39	− 0.4	37.8	21.27	8.18	0.38
	RH_{mean} (%)	19.5	99	79.19	10.29	0.13	23.5	100	77.61	10.9	0.14
	P (mm)	0	115.2	3.68	9.78	2.65	0	102.4	4.15	11.91	2.86
	SSH (hr)	0	12.5	5.01	4.13	0.82	0	12.5	5.2	4.33	0.83
	W (m/s)	0	25	4.42	2.65	0.59	0	20	4.92	2.28	0.46
	e_s-e_a (KPa)	0.01	2.65	0.49	0.37	0.76	0	2.02	0.54	0.42	0.77
	R_S (MJ m^{-2} day^{-1})	1.17	17.77	7.81	4.58	0.58	1.95	17.82	7.93	4.83	0.6
	E_{pan} (mm day^{-1})	0.2	10	2.64	2.16	0.81	0.2	10	2.88	2.4	0.83

2.2.2 Krill herd algorithm (KHA)

Krill herd algorithm (KHA) is a bio-inspired optimization algorithm according to Krill herd real behavior in nature. This novel metaheuristic population-based algorithm was proposed by Gandomi and Alavi (2012) for solving optimization problems. The inspiration behind the selection of KHA algorithm is simulation behavior of Krill when they are looking for the nearest food (Abualigah et al. 2017).

Objective function includes minimum distance of each krill from food and the highest density of herd, ultimately leading them to swarm around the global optimum. During the process, Krill search for food, while the highest density of herd move toward the best solution. Krill herd algorithm illustrates

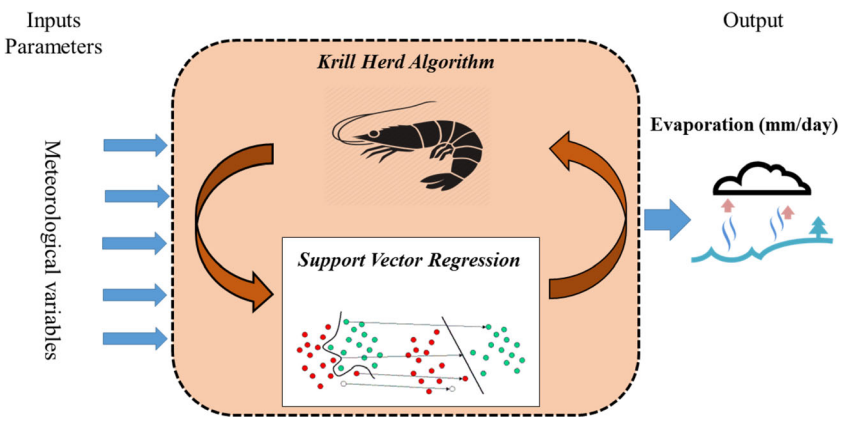

Fig. 3 Schematic structure of the SVR-KHA method for evaporation prediction

the following Lagrangian model (Eq. 5) in n-dimensional decision space:

$$\frac{dX_i}{dt} = N_i + F_i + D_i \quad (3)$$

where Ni, Fi, and Di are the motion vectors induced by other krill individuals, foraging movement, and physical diffusion of the i_{th} krill, respectively. Direction of motion induced by other krill (αi) is estimated from local effect, target effect, and repulsive effect. For the i_{th} Krill, this motion is defined by Eq. 6.

$$N_i^{new} = N^{max}\alpha_i + \omega_n N_i^{old} \quad (4)$$

where N^{max} is a maximum induced speed, ω_n is the inertia weight of induced motion in the range (0,1) and N_i^{old} is the last induced-motion. Figure 4 shows modeling flowchart of the SVR-KHA used in the present study.

2.3 Model implementation and scenario selection

In the current study, several simple SVR and SVR-KHA hybrid models are developed for estimation of E_{pan}, each one considering a different combination of predictor variables. Selection of appropriate predictor variables is one of the crucial steps in modeling of hydro-meteorological datasets accurately. Therefore, the most important parameters including maximum temperature (T_{max}), mean relative humidity (RH_{mean}), precipitation (mm), sunshine hours (SSH), wind speed (W), difference between saturation and actual vapor pressure (es-ea), and radiation (Rs) are considered based on previous literature for estimation of E_{pan}. During the analyses, statistical cross-correlations between different variables at different locations are computed first, which are presented in Table 3.

Table 3 presents that E_{pan} shows a strong positive correlation (say > 0.6) with T_{max}, (es-ea), R_s, and SSH, while it shows a negative correlation with average relative humidity (RH_{mean}) and precipitation (P) at all the stations considered in this study. Evaporation shows a reasonably good positive correlation (0.623) with wind speed at Osku station, however, showing very weak correlation with wind speed (0.086 and 0.232) at other two stations. The latter two stations are located at the coast, while the former one (Osku) is situated in the interior geographical stretch. It should also be noted that Osku station is located at much higher altitude (1428 m) when compared with the other two (Table 1). Therefore, geographical and meteorological characteristics of Osku station are quite different from that of the other two stations. A close examination further shows that there exists a similarity in the correlation between different variables of the two coastal stations, Bandar Abbas and Rudsar. The nature of mutual correlation between different variables is quite different for Osku station when compared with the other two stations. Seven different combinations of input variables are considered for SVR and SVR-KHA hybrid-based modeling, which is listed in Table 4.

This study developed the standalone SVR and the SVR-KHR model for different scenarios. Hence for each station, a total of 14 different models were developed for estimation of pan evaporation. The performance assessment is carried out using multitude of statistical measures and graphical tools.

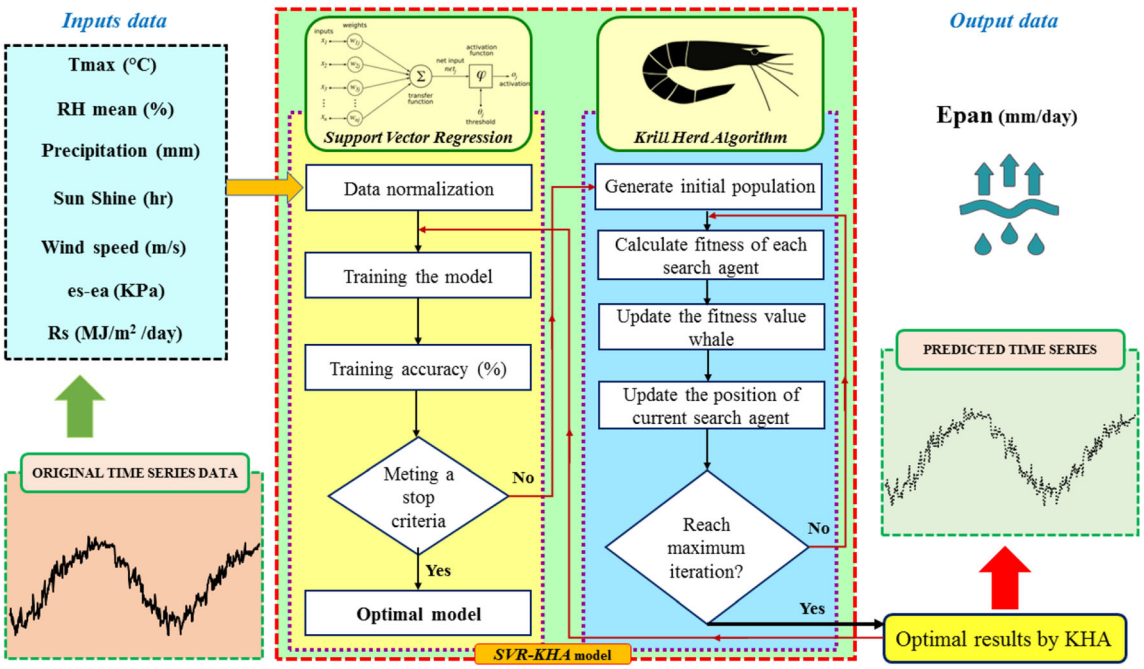

Fig. 4 Flowchart of the hybrid Krill herd algorithms coupled with support vector regression (SVR-KHA) used in current study

Table 3 Cross-correlation between predictor variables of three stations in Iran (**a**) Bandar Abbas, (**b**) Osku, and (**c**) Rudsar

Variable	Tmax	RHavg	P	SSH	W	(es-ea)	Rs	E
(a) Bandarabbas station								
T_{max}	1	− 0.540	− 0.223	0.603	0.019	0.839	0.792	0.781
RH_{mean}		1	0.329	− 0.630	− 0.186	− 0.821	− 0.457	− 0.574
P			1	− 0.293	0.283	− 0.252	− 0.223	− 0.216
SSH				1	− 0.058	0.656	0.750	0.665
W					1	0.125	0.000	0.086
(es-ea)						1	0.736	0.814
R_s							1	0.832
E_{pan}								1
(b) Osku station								
T_{max}	1	− 0.532	− 0.178	0.622	0.487	0.884	0.789	0.814
RH_{mean}		1	0.227	− 0.462	− 0.121	− 0.747	− 0.321	− 0.490
P			1	−0.355	− 0.020	− 0.190	− 0.166	− 0.171
SSH				1	0.321	0.571	0.703	0.626
W					1	0.428	0.647	0.623
(es-ea)						1	0.695	0.845
R_s							1	0.849
E_{pan}								1
(c) Rudsar station								
T_{max}	1	− 0.568	− 0.199	0.583	0.129	0.845	0.787	0.782
RH_{mean}		1	0.360	− 0.674	− 0.304	− 0.830	− 0.469	− 0.612
P			1	− 0.337	0.082	− 0.263	− 0.230	− 0.268
SSH				1	0.240	0.647	0.710	0.706
W					1	0.229	0.176	0.232
(es-ea)						1	0.730	0.821
R_s							1	0.855
E_{pan}								1

2.4 Assessment criteria

Seven metrics were applied to evaluate the ability of each predictor model. These metrics include root-mean-square error (RMSE), mean absolute error (MAE), Wilmot-index (WI), mean absolute percent error (MAPE), coefficient of determination (R^2), Relative Root Mean Square Error (RRMSE), and Mean Absolute Relative Error (MARE) as in the following equations:

Table 4 Input combinations and models for prediction of Pan evaporation

Scenario	Input parameters	Support vector regression	Krill herd hybrid algorithm
1	T_{max}	SVR1	SVR-KHA1
2	T_{max}, RH_{mean}	SVR2	SVR-KHA2
3	T_{max}, RH_{mean}, precipitation	SVR3	SVR-KHA3
4	T_{max}, RH_{mean}, precipitation, sun shine hours	SVR4	SVR-KHA4
5	T_{max}, RH_{mean}, precipitation, sun shine, wind speed	SVR5	SVR-KHA5
6	T_{max}, RH_{mean}, precipitation, sun shine hours, wind speed, es-ea	SVR6	SVR-KHA6
7	T_{max}, RH_{mean}, precipitation, sun shine hours, wind speed, es-ea, R_s	SVR7	SVR-KHA7

$$RMSE = \sqrt{\frac{\left(\sum_{i=1}^{N}\left(x_i - \overline{y}\right)^2\right)}{N}} \quad (5)$$

$$MAE = \frac{\sum(|x_i - y_i|)}{n} \quad (6)$$

$$WI = 1 - \frac{\sum(x_i - y_i)^2}{\sum\left(\left|y_i - \overline{x}\right| + \left|x_i - \overline{x}\right|\right)^2} \quad (7)$$

$$MAPE = \frac{1}{\overline{x}}\frac{\sum|x_i - y_i|}{n} \times 100 \quad (8)$$

$$R^2 = \left(\frac{1}{n} \times \frac{\sum\left(x_i - \overline{x}\right)\left(y_i - \overline{y}\right)}{(\sigma_x)(\sigma_y)}\right)^2 \quad (9)$$

$$RRMSE = \frac{\sqrt{\frac{1}{n}\sum_{i=1}^{n}(x_i - y_i)^2}}{\sum_{i=1}^{n} x_i} \times 100 \quad (10)$$

$$MARE = \frac{\sum\left(\frac{|x_i - y_i|}{x_i}\right)}{n} \quad (11)$$

where x_i is the observed value, $\overline{x}$ is the mean of observed values, y_i is the estimated value, $\overline{y}$ is the mean of estimated values, σx and σy are the standard deviations of the observed and estimated data, and n is the number of observations. Apart from the above, Bayesian Information Criteria (BIC) is used to select the best scenario. Also the scatter plots, residual plot (error plot), box plots, and histograms were used as graphical tools for the selection of the best model for the estimation of E_{pan} of the three stations.

3 Results

In the modeling phase, for each scenario presented in Section 2.3, both SVR and SVR-KHA hybrid models were developed. In both SVR and SVR-KHA hybrid modeling, the initial 70% of data of each station are considered to be training dataset, while the remaining 30% of data as a testing dataset. The performance of different models is compared by using a set of assessment criteria presented in Section 2.4. The results of performance evaluation statistics for Bandar Abbas, Osku, and Rudsar stations are presented in Table 5, Tables 6 and 7, respectively. The higher value of R^2 and WI (close to 1) and lower value of different error measures (like RMSE, MAE, RRMSE, and MARE) indicate better performance. From Table 5, it is noted that inclusion of additional parameters results in a consistent improvement in the performance of E_{pan} estimation model. Also, all the KHA hybrid variants consistently show better performance as compared with their simple SVR counterparts. SVR7 model, which considers seven important meteorological variables (T_{max}, RH_{mean}, precipitation (P), sun shine hours (SSH), wind speed (W), (es-ea), and radiation (Rs)), shows the best performance among different SVR models. Along with the combination of variables, the influence of KHA hybridization is also examined. The single input (T_{max}) SVR1 model hybrid with KHA (hereinafter, SVR-KHA1) shows an improved performance (R^2 of 0.717 and RMSE of 1.032) as compared with multi-input SVR models, e.g., SVR5 (with RMSE and MAE of 1.037 and 0.773). However, SVR6 and SVR7 models show significantly better performance as compared with the first three hybrid SVR models. This demonstrates that the mere inclusion of additional parameters will not help in improving model performance rather it may complicate the modeling. On the other hand, KHA hybridization will improve the performance even with less number of predictor variables. The two higher-order models SVR6 and SVR7 show good performance in prediction of daily E_{pan} with marginally better performance for SVR7 model. Hybridizing these models with KHA consistently results in better performance. SVR7 model hybridized with KHA (SVR-KHA7) shows best performance among the different models considered in this study for modeling E_{pan} at Bandar Abbas station. A careful perusal of statistics presented in Tables 6 and 7 show that identical comments on the performance of different models hold good for the results of Osku and Rudsar stations.

The Bayesian Information Criterion (BIC), also known as Schwarz Criterion (SC), was developed by Gideon Schwarz. BIC is used as a criterion for selection of most suitable model and for the comparative evaluation of different time series models (Schwarz 1978). The BIC is partly based on likelihood function and very closely related to Akaike Information Criterion (AIC). The main difference between BIC and AIC is manifested when more parameters or variables are added in order to increase goodness of fit. The BIC introduces a penalty term for the number of parameters in each model. This penalty term is higher in BIC as compared with AIC. The minimum BIC value represents lower penalty term and best model performance (Schwarz 1978).

In the current study, BIC is applied to each model under consideration including classical SVR and hybrid SVR-KHA models. BIC is checked during both training and testing periods at the selected three stations. Table 8 shows that the model performance increases generally with increase in number of parameters both in training and testing periods. The results show that SVR6 is the best model at Bandar Abbas station during training period with BIC values of 29.16, while SVR5 is the optimal model during training period with 114.5

Table 5 Performance evaluation of different E_{pan} estimation models at Bandar Abbas station. (The bold figures show the performance statistics of the best model)

Models	RMSE	MAE	WI	MAPE	R^2	RRMSE	MARE
(a) Training phase							
SVR1	1.239	0.928	0.846	79.289	0.588	51.734	0.793
SVR2	1.177	0.877	0.868	74.592	0.627	49.134	0.746
SVR3	1.177	0.876	0.869	74.338	0.626	49.164	0.743
SVR4	1.121	0.830	0.883	70.548	0.662	46.833	0.705
SVR5	1.115	0.825	0.885	69.847	0.666	46.562	0.698
SVR6	0.997	0.690	0.918	52.784	0.733	41.615	0.528
SVR7	0.915	0.615	0.933	48.104	0.774	38.223	0.481
SVR-KHA1	1.106	0.791	0.892	65.278	0.667	46.194	0.653
SVR-KHA2	1.032	0.728	0.91	57.067	0.711	43.096	0.571
SVR-KHA3	1.027	0.724	0.91	56.534	0.713	42.885	0.565
SVR-KHA4	0.985	0.687	0.919	54.927	0.737	41.116	0.549
SVR-KHA5	0.973	0.676	0.921	54.425	0.743	40.628	0.544
SVR-KHA6	0.941	0.652	0.927	53.669	0.759	39.293	0.537
SVR-KHA7	**0.884**	**0.599**	**0.938**	**50.139**	**0.788**	**36.908**	**0.501**
(b) Testing phase							
SVR1	1.142	0.851	0.872	56.013	0.675	45.377	0.56
SVR2	1.097	0.824	0.891	58.205	0.689	43.593	0.582
SVR3	1.101	0.826	0.891	58.508	0.686	43.748	0.585
SVR4	1.042	0.783	0.903	56.413	0.719	41.414	0.564
SVR5	1.037	0.773	0.904	54.685	0.724	41.200	0.547
SVR6	0.924	0.655	0.934	40.785	0.776	36.730	0.408
SVR7	0.831	0.583	0.948	36.386	0.819	33.033	0.364
SVR-KHA1	1.032	0.735	0.91	46.758	0.717	40.984	0.468
SVR-KHA2	0.975	0.682	0.924	43.949	0.747	38.719	0.439
SVR-KHA3	0.953	0.669	0.927	43.195	0.757	37.871	0.432
SVR-KHA4	0.913	0.644	0.935	41.095	0.778	36.272	0.411
SVR-KHA5	0.902	0.635	0.937	41.179	0.783	35.842	0.412
SVR-KHA6	0.878	0.62	0.941	40.133	0.795	34.875	0.401
SVR-KHA7	**0.784**	**0.564**	**0.955**	**36.912**	**0.836**	**31.155**	**0.369**

BIC. Similarly, SVR7 outperformed all other classic SVR models at Osku and Rudsar stations with 2902.74 and − 3.344 BIC values during training period. However, SVR7 and SVR6 are the best models during testing phase at Osku and Rudsar stations.

Among the hybrid models (SVR-KHA), the optimal models during training periods are SVR-KHA4 (− 48.28), SVR-KHA7 (1757.15), and SVR-KHA5 (− 44.32) at Bandar Abbas, Osku, and Rudsar stations, respectively. On the other hand, SVR-KHA2 (− 42.53), SVR-KHA7 (1039.39), and SVR-KHA4 (− 6.87) are the best models during the testing period. Overall, the model performance is getting higher with increase in number of input variables. The performance of hybrid models is significantly improved as compared with their respective classic models.

Figure 5 shows a scatter plot of estimated E_{pan} based on SVR7 and SVR-KHA7 at three stations during testing period (2016–2018). The scatter plots show that estimation at Bandar Abbas and Rudsar stations by SVR and SVR-KHA are similar, with similar R^2 statistics values of 0.82 and 0.84 at Bandar Abbas station and 0.88 and 0.9 at Rudsar station, respectively. The pattern of estimated E_{pan} was also found to be similar in these two cases. However, the improvement in performance of E_{pan} estimation by SVR-KHA7 model as compared with SVR7 model is more perceptible for Osku station (with R^2 of 0.91 and 0.86, respectively). This could also be linked with the unique role of different meteorological data of Osku station as compared with the other two coastal stations. E_{pan} shows a strong positive correlation (> 0.6) with $T_{max,}$ (es-ea), R_s and SSH, and negative correlation with RH_{mean} and P irrespective of the stations (Table 3). A reasonably good

Table 6 Performance evaluation of different E_{pan} estimation models at Osku station. (The bold figures show the performance statistics of best model)

Models	RMSE	MAE	WI	MAPE	R^2	RRMSE	MARE
(a) Training phase							
SVR1	2.815	2.207	0.881	61.048	0.662	43.268	0.61
SVR2	2.791	2.199	0.885	61.535	0.666	42.903	0.615
SVR3	2.787	2.199	0.887	61.961	0.666	42.841	0.62
SVR4	2.711	2.143	0.893	61.843	0.685	41.672	0.618
SVR5	2.401	1.838	0.921	52.391	0.754	36.914	0.524
SVR6	1.905	1.392	0.956	35.693	0.843	29.28	0.357
SVR7	1.745	1.266	0.964	32.013	0.868	26.828	0.32
SVR-KHA1	2.499	1.842	0.917	45.477	0.730	38.41	0.455
SVR-KHA2	2.438	1.789	0.921	44.608	0.743	37.47	0.446
SVR-KHA3	2.409	1.765	0.924	43.058	0.749	37.037	0.431
SVR-KHA4	2.111	1.551	0.944	38.138	0.807	32.455	0.381
SVR-KHA5	1.752	1.255	0.963	29.572	0.867	26.933	0.296
SVR-KHA6	1.473	1.064	0.975	27.223	0.906	22.648	0.272
SVR-KHA7	**1.395**	**1.005**	**0.978**	**25.796**	**0.916**	**21.443**	**0.258**
(b) Testing phase							
SVR1	2.882	2.297	0.873	54.528	0.663	41.487	0.545
SVR2	2.849	2.282	0.878	54.295	0.669	41.013	0.543
SVR3	2.84	2.279	0.88	54.555	0.669	40.885	0.546
SVR4	2.764	2.217	0.886	54.31	0.690	39.789	0.543
SVR5	2.459	1.876	0.916	42.672	0.781	35.389	0.427
SVR6	2.094	1.534	0.946	32.289	0.830	30.140	0.323
SVR7	1.849	1.367	0.959	27.374	0.865	26.613	0.274
SVR-KHA1	2.566	1.924	0.913	40.557	0.724	36.94	0.406
SVR-KHA2	2.526	1.887	0.916	39.54	0.733	36.365	0.395
SVR-KHA3	2.491	1.866	0.919	39.076	0.742	35.862	0.391
SVR-KHA4	2.317	1.744	0.931	38.758	0.776	33.348	0.388
SVR-KHA5	1.987	1.419	0.951	28.221	0.851	28.603	0.282
SVR-KHA6	1.685	1.215	0.967	25.44	0.889	24.257	0.254
SVR-KHA7	**1.517**	**1.117**	**0.974**	**23.41**	**0.911**	**21.834**	**0.234**

correlation (0.623) of E_{pan} with wind speed is observed at Osku station, against very weak correlation (0.086 and 0.232) between these variables at Bandar Abbas and Rudsar stations. The scatter plots also depict that the deviations from the idea fit are less for the prediction by SVR-KHA7 when compared with that by SVR7 model. In order to get a clear picture of bias (deviation) of predictions, the residual plots were prepared for testing datasets at all three stations and presented in Fig. 6. The graphical comparison of residuals shows that more deviation is observed in SVR7 model when compared with its respective KHA hybrid model at all the stations. For example, the residuals are constrained between −3.0 and 3.0 for the SVR-KHA7 model of Bandar Abbas station, on the other hand, the residuals are larger in magnitude and show many spikes for the SVR7 model. Similarly, for Osku station data, residual magnitudes of SVM-KHA7 are relatively uniform in pattern and centered around the neural line. However, localized larger magnitude residuals (as high as 8 mm) are observed in the predictions by SVM7 models. The magnitude of residuals for SVR-KHA7 model are mostly in the range of −2 to 2 mm at Rudsar station; however, SVR7 model resulted in numerous high-magnitude residual indicated by abundance in spikes in the residual plot. In general, the SVR-KHA7-based predictions are more consistent with stable residuals of lesser magnitude as compared with SVR7-based predictions.

Furthermore, the box plots are prepared to decipher the predictability potential (accuracy) of the SVR-KHA7 model in comparison with other KHA models (Fig. 7). A comparison of the box plots shows that the mean and median of predictions by SVR6 and SVR7 and their hybrid counterparts match significantly with the statistics of the observed dataset. The figure shows that the IQR ranges of predictions by SVR-KHA7 model match well with the observed data of Bandar

Table 7 Performance evaluation of different E_{pan} estimation models at Rudsar station (the bold figures show the performance statistics of the best model)

Models	RMSE	MAE	WI	MAPE	R^2	RRMSE	MARE
(a) Training phase							
SVR1	1.39	1.054	0.854	92.493	0.591	52.529	0.925
SVR2	1.322	1.011	0.871	88.808	0.629	49.991	0.888
SVR3	1.319	1.008	0.87	87.838	0.633	49.862	0.878
SVR4	1.218	0.938	0.894	81.599	0.686	46.049	0.816
SVR5	1.206	0.92	0.896	78.292	0.694	45.572	0.783
SVR6	1.085	0.771	0.926	56.255	0.751	41.004	0.563
SVR7	0.989	0.690	0.941	51.012	0.793	37.372	0.510
SVR-KHA1	1.243	0.899	0.894	75.718	0.670	47.005	0.757
SVR-KHA2	1.142	0.816	0.914	63.477	0.722	43.165	0.635
SVR-KHA3	1.099	0.788	0.922	58.682	0.742	41.562	0.587
SVR-KHA4	1.022	0.738	0.934	55.949	0.777	38.624	0.559
SVR-KHA5	0.984	0.702	0.939	52.357	0.794	37.188	0.524
SVR-KHA6	0.977	0.700	0.94	52.597	0.796	36.933	0.526
SVR-KHA7	**0.922**	**0.652**	**0.948**	**49.791**	**0.819**	**34.868**	**0.498**
(b) Testing phase							
SVR1	1.472	1.098	0.855	64.498	0.664	51.083	0.645
SVR2	1.364	1.03	0.882	61.654	0.706	47.332	0.617
SVR3	1.371	1.039	0.88	61.399	0.708	47.567	0.614
SVR4	1.246	0.95	0.905	56.478	0.763	43.223	0.565
SVR5	1.264	0.96	0.900	57.56	0.758	43.865	0.576
SVR6	1.018	0.721	0.947	39.508	0.826	35.305	0.395
SVR7	0.855	0.598	0.964	32.852	0.877	29.650	0.329
SVR-KHA1	1.299	0.926	0.900	54.517	0.723	45.056	0.545
SVR-KHA2	1.158	0.830	0.925	44.619	0.777	40.179	0.446
SVR-KHA3	1.13	0.807	0.929	43.392	0.788	39.204	0.434
SVR-KHA4	0.984	0.703	0.948	38.911	0.842	34.147	0.389
SVR-KHA5	0.99	0.708	0.947	41.688	0.841	34.338	0.417
SVR-KHA6	0.952	0.678	0.952	41.016	0.850	33.046	0.41
SVR-KHA7	**0.784**	**0.571**	**0.969**	**35.158**	**0.900**	**27.203**	**0.352**

Abbas station. Similarly, the IQR range of predictions by SVR7, SVR-KHA7, and SVR-KHA6 models matches well with that of observed data of Osku station. The range of predictions shows that SVR6 and SVR7 traditional models result in high over predictions than their KHA hybrid variants. Moreover, it is noted that the performance of SVR-KHA7 and SVR-KHA6 models is strikingly similar for the predictions at this station. For Rudsar station, the IQR range of SVR-KHA7 closely matches that of an observed dataset. The ranges of values also match reasonably well for SVR6, SVR7, and the SVR-KHA7 model.

In order to get a better understanding of the prediction accuracies of two competing models, SVR7 and SVR-KHA, E_{pan} values of diverse ranges, observations, and predictions in different ranges are compared. Histograms of the estimated and observed E_{pan} values are presented in Fig. 8. The subplots in Fig. 8 represent the probability occurrence of E_{pan} within a specific range (Al-Shammari et al. 2016). The estimation of E_{pan} at Bandar Abbas station depicts that for the lowest (1–3 mm) and the highest (7–9 mm) ranges of E_{pan}, the frequency (number of days) of accurate estimation by SVR-KHA7 model shows better agreement with the frequency of observed values as compared with the frequency of accurate estimates by SVR7 model. The performance of both models (SVR-KHA7 and SVR7) is quite similar for middle range values (3–5 mm); however, a marginal improvement is noted in the performance of SVR-KHA7 model over SVR-7 model. Comparison based on the frequency of predictions of E_{pan} at Osku stations revealed better predictions of SVR-KHA7 model as compared with SVR7 model. The difference in the frequency of various data ranges is smaller in the SVR-KHA7-based predictions as compared with SVR7 model.

Table 8 Evaluation of BIC index according to number of model inputs

Models	Number of inputs	Bandar Abbas		Osku		Rudsar	
		Training	Testing	Training	Testing	Training	Testing
SVR1	1	1102.99	297.94	5300.11	2325.27	1690.48	854.24
SVR2	2	847.19	217.1	5264.54	2307.13	1445.13	694.2
SVR3	3	858.14	231.9	5265.07	2307.26	1439.77	712.06
SVR4	4	617.6	118.8	5131.4	2254.78	1040.72	509.32
SVR5	5	595.71	114.5	4519.18	2005.09	995.3	548.6
SVR6	6	29.16	−130.01	3342.25	1660.53	463.1	80.16
SVR7	7	−397.85	−355.39	2902.74	1395	−3.44	−295.13
SVR-KHA1	1	523.8	74.99	4691	2071.05	1122.26	579.3
SVR-KHA2	2	176.54	−42.53	4572.22	2043.69	694.33	335.41
SVR-KHA3	3	159.3	−84.02	4520.62	2020.18	508.59	288.59
SVR-KHA4	4	−48.28	−171.5	3852.97	1868.03	141.58	−6.87
SVR-KHA5	5	−101.48	−190.6	2907.12	1538.87	−44.32	12.37
SVR-KHA6	6	−264.47	−243.51	2028.7	1185	−71.72	−64.63
SVR-KHA7	7	−576.92	−410.11	1757.15	1039.39	−358.12	−283.07

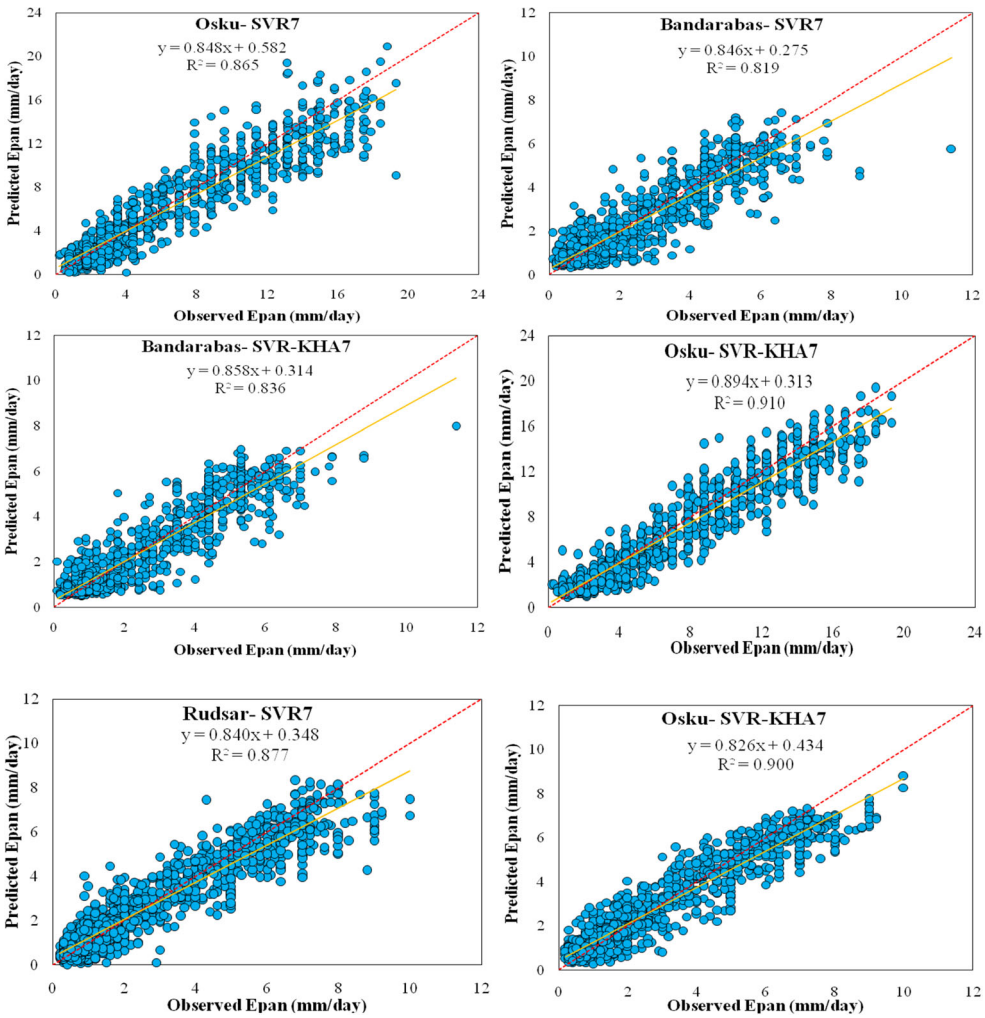

Fig. 5 Scatter plot of best scenario for SVR and SVR-KHA models in the testing period

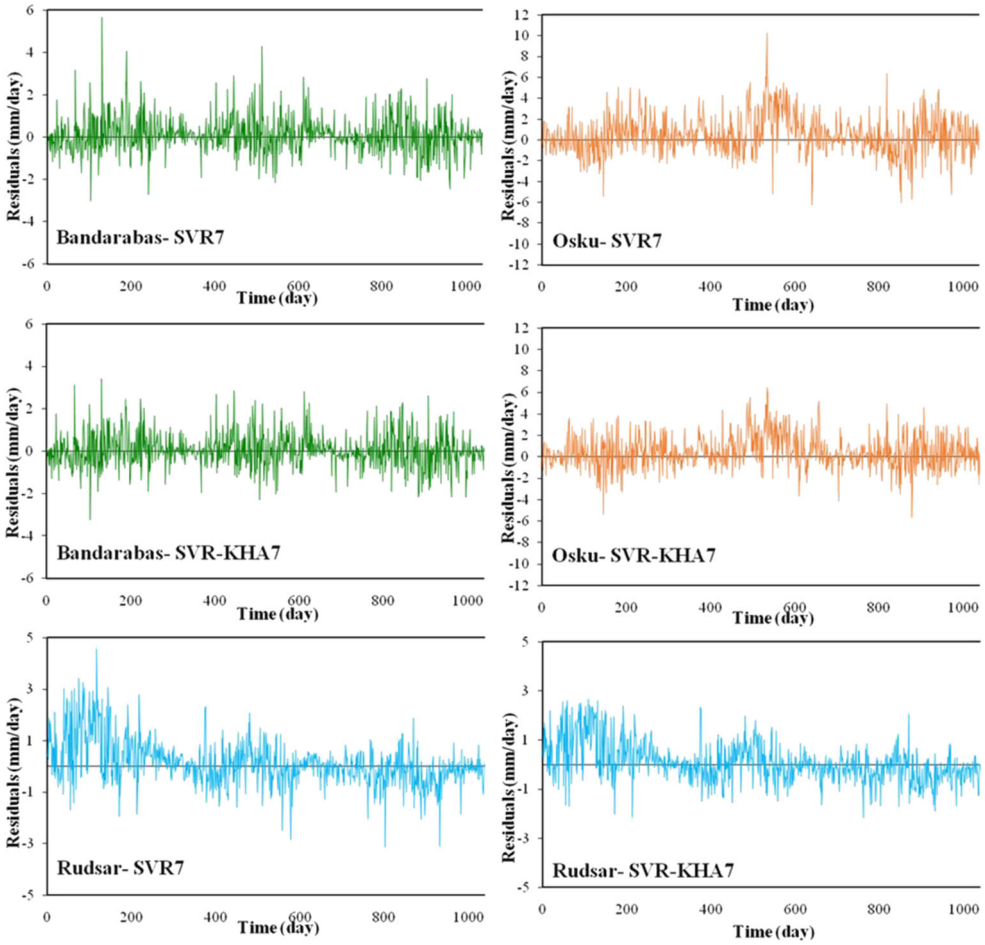

Fig. 6 The residual (error plot) of the best ordinary SVR and the hybrid SVR-KHA, for testing period

Also, it is noted that the SVR-7 model, resulted in over predictions in the range of higher E_{pan} values (exceeding 21 mm). Moreover, at Rudsar station, the comparison of prediction frequency in different ranges revealed the marginal improvements of SVR-KHA7 model. In general, the histogram plots show that during the testing period, the probability distribution of the predicted data is closer to that of the observed data in SVR-KHA models (better agreement) than the corresponding standalone SVR models. The setting of model parameters is important aspect in hydrological modeling (Mohammadi 2019a, b), and providing model details will be helpful for future potential researchers (Mohammadi 2020). In the current study, the SVR optimal parameters are fixed by trial and error method. The optimal parameters of SVR, i.e., radial basis function parameter and trade-off parameter are ranging between 0.3–16.4 and 1.54–13.67, respectively. Furthermore, 500 maximum numbers of simulations and 40 numbers of krills with 0.02 velocity of foraging and 0.01 maximum induced speed are used to run the KHA model. However, this model needs to be applied for other regions around the globe based on criteria/inputs specified in the research.

4 Discussion

In recent year, researchers are now focusing on application of machine learning techniques in different fields such as hydrology, soil sciences, hydrologic modeling, and water resources management (Mohammadi and Mehdizadeh 2020; Mohammadi et al. 2020; Jahani and Mohammadi 2019; Vaheddoost et al. 2020; Ghorbani et al. 2018; Pham et al. 2020; Moazenzadeh et al. 2018). Several machine learning algorithms and models are developed to estimate the E_{pan}, such as ANN, SVM, ANFIS, GNN, MLP, ELM, ENN, CCNN, and much more. The machine learning models are proved more robust, simple, and accurate as compared with other traditional indirect methods in estimation of E_{pan}.

Very recently, Majhi and Naidu (2020) estimated E_{pan} using Functional Link Artificial Neural Network (FLANN) model across three agro-climatic regions of Chhattisgarh state in east-central India. The FLANN model was also compared with Multi-Layer Artificial Neural Network (MLANN). The results showed that FLANN model estimated the E_{pan} with high accuracy (RMSE = 0.85–1.27 mm/day and MAE = 0.63–0.95 mm/day) as compared with MLANN (RMSE = 0.94–1.58 mm/day and MAE = 0.73–1.14 mm/day). Wang et al. (2020) estimated E_{pan} using a new hybrid model based

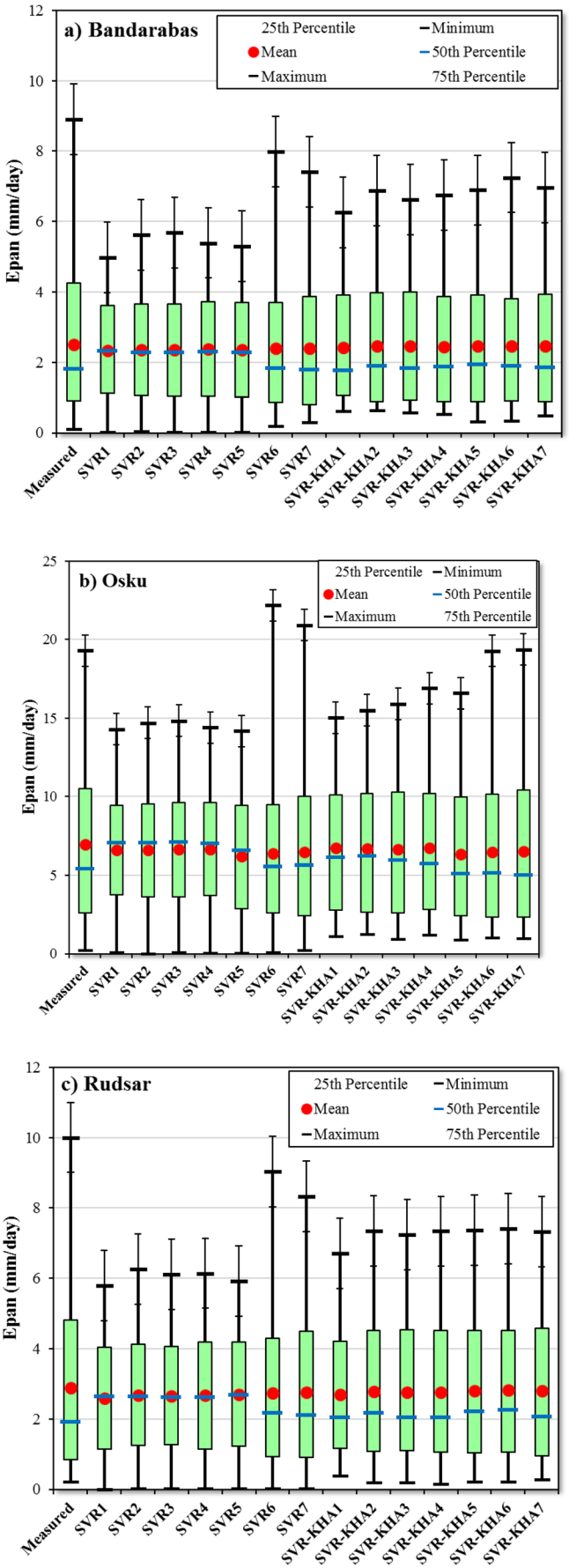

Fig. 7 Box plots of predictions of E_{pan} of different stations for the testing period (**a**) Bandar Abbas, (**b**) Osku, (**c**) Rudsar

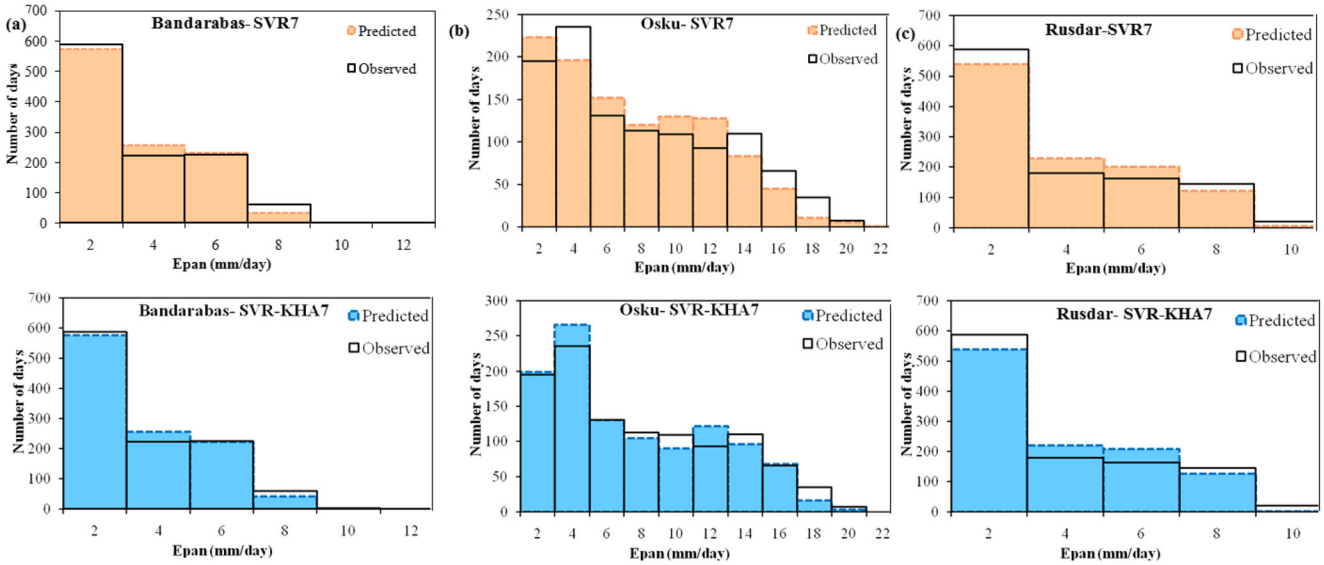

Fig. 8 The histogram of the simulated and the observed E_{pan} of the optimal standalone and the hybrid models (SVR7 and SVR-KHA7) for the study areas during the testing period

on Slap Swarm Algorithm (SSA) and Kernel-based Nonlinear Arps Decline (KNEA). The hybrid model was also compared with M5 model tree (M5) and Multivariate Adaptive Regression Splines (MARS) models across the arid and semi-arid regions of north-west China. The results demonstrated that KNEA model outperformed the M5 and MARS model. The average RMSE and MAE values for KNEA model are 1.067 mm/day and 0.867 mm/day.

Wu et al. (2020) compared the extreme learning machine (ELM) model with two new meta-heuristic algorithms including whale optimization algorithm (WOA) and flower pollination algorithm (FPA) to estimate monthly E_{pan} across Poyang Lake Basin of Southern China. Moreover, they also developed two hybrid models, i.e., WOAFLM and FPAELM and the Differential Evolution algorithm optimized ELM (DEELM). The results reported better performance of hybrid models (WOAFLM and FPAELM) as compared with DEELM in the first scenario (only considering temperature as input). The RMSE, MAE, and MAPE for DEELM was 4.5%, 4.8%, and 5.3% higher than WOAFLM and FPAELM, respectively, during testing period. The error statistics of FPAELM and WOAFLM were close to each other and the performance increased with increase in number of input variables. The average RMSE, MAE, MAPE, and R^2 of FPAELM model across the study area are 0.2038 mm/day, 0.1576 mm/day, 0.0663, and 0.962, respectively. Similarly, the results for WOAFLM models are 0.2036 mm/day, 0.1573 mm/day, 0.0663, and 0.963, respectively. Majhi et al. (2019) estimated E_{pan} using deep neural network architecture with long short-term memory cell (Deep-LSTM). The Deep-LSTM model was also compared with MLANN and empirical methods, i.e., Hargreaves and Blaney-Criddle. The results demonstrated that both Deep-LSTM and MLANN models can precisely estimate daily E_{pan} with high accuracy. Moreover, Deep-LSTM model outperformed all the empirical models and MLANN. The high performance of Deep-LSTM is verified using several statistical metrics and AIC.

Lu et al. (2018) estimated E_{pan} using four empirical and three tree-based machine learning models at local (target station) and cross-station data across Poyang Lake watershed of China. The models include M5 model tree (M5tree), random forests (RFs), and gradient boosting decision tree (GBDT). The results demonstrated the best performance of radiation-based Priestly-Taylor model with average RMSE = 1.13 mm/day, MBE = 0.21 mm/day, and $R^2 = 0.57$. On the other hand, mass transfer-based Trabert model performed worst with RMSE = 1.38 mm/day, MBE = 0.65 mm/day, and $R^2 = 0.46$. The GBDT outperformed all the models with RMSE = 0.86 mm/day, MBE = 0.07 mm/day, and $R^2 = 0.73$. Moreover, a distance of less than 100 km is recommended for cross-section application with satisfactory results and accuracy.

Wang et al. (2017c) simulated E_{pan} using MLP, GRNN, FG, LSSVM, MARS, ANFIS-GP, and two regression models, i.e., MLR and SS. The results demonstrated that the accuracy of all models is dependent on the geography and climate of the region. MLP model outperformed all other models at HEB station with average MAE, RMSE, and R^2 values of 0.314 mm/day, 0.405 mm/day, and 0.988, respectively. While the GRNN model presented significantly better performance in Tibetan Plateau with average MAE, RMSE, and R^2 values 0.459 mm/day, 0.592 mm/day, and 0.932, respectively.

Kisi (2015) evaluated the precision of least square support vector machine (LSSVM), MARS, and M5 models to estimate the E_{pan} at the Mersin and Antalya stations situated in the Mediterranean region of Turkey. LSSVM model outperformed M5 and MARS models with 24–32.1% and 10.8–18.9% improvements in RMSE as compared with RMSE of M5 and MARS models at Mersim and Antalya stations, respectively. Moreover, the accuracies of these models are also tested using solar radiation, air temperature, relative humidity, and wind speed as input data from nearby stations (cross-station application). The results demonstrated better accuracy of MARS model as compared with LSSVM and M5 models. The accuracy of LSSVM and M5 are increased by 3.7% and 16.5% using average RMSE as a criterion. During the cross-station application, the average RMSE accuracy of LSSVM and M5 models are increased by 11.4% and 18.4%, respectively.

All the above-mentioned studies are consistent with the current study; depicting the performance of machine learning-based models are dependent on the number of input variables and whether model is a hybrid model or standalone model. The results of the previous studies and current research demonstrate significant improvement in model performance when the number of input variables is increased. The hybrid models have higher performance even the input variables are much less as compared with standalone models. For example, in the current study, a single input model (SVR1) combined with KHA (SVR-KHA1) has high performance with R^2 of 0.717 and RMSE of 1.032 as compared with SVR5 having RMSE and R^2 of 1.037 and 0.66, respectively. Overall, the results confirmed the best performance of SVR-KHA models as compared with SVR standalone model, which is supported by previous studies (Wang et al. 2017c, 2020; Wu et al. 2020; Majhi et al. 2019).

5 Conclusions

In this study, several classical SVR models and SVR hybrid models coupling with Krill Herd (KH) algorithm are developed for prediction of daily pan evaporation (E_{pan}) across the three stations Bandar Abbas, Osku, and Rudsar located at coastal region of Iran.

The study revealed that the performance of classical and hybrid models increased with increase in number of parameters. The best performing models are comprised of seven meteorological input variables including maximum temperature (T_{max}), difference between saturation and actual vapor pressure (es-ea), radiation (R_s), sunshine hours (SSH), average relative humidity (RH_{mean}), precipitation (P), and wind speed (W).

E_{pan} estimates at the two coastal stations of Bandar Abbas and Rudsar by SVR and SVR-KHA methods are found to be similar but higher improvements are observed in the E_{pan} estimates at Osku station (with R^2 of 0.91 and 0.86, respectively by SVR-KHA and simple SVR model).

The estimation of E_{pan} by the SVR-KHA model is found to be the most reliable at the geographically interior and high altitude Osku station than the other two coastal stations. This could be attributed to the impact of the dominant role of wind speed on the process of E_{pan} at the Osku station and the interplay between the complementary meteorological variables on the process at the other two stations.

The study considered different combination of predictor variables for the prediction of E_{pan}, i.e., increasing the model complexity by systematic addition of input variables. Single input SVR1 model hybrid with KHA (SVR-KHA1) showed improved performance (R^2 of 0.717 and RMSE of 1.032) as compared with multi-input SVR models, e.g., SVR5 (with RMSE and MAE of 1.037 and 0.773). This shows that inclusion of more meteorological parameters may not improve the performance of standalone SVR model, but the use of KHA shows improvements in estimation, even with less number of input parameters. The results show that the SVR-KHA models perform better than standalone SVR models in prediction of E_{pan} of the three stations in all cases with stable residuals of lower magnitude and better statistical performance evaluation measures.

The SVR7 model hybridized with KHA (SVR-KHA7), which considers all the seven meteorological inputs (T_{max}, RH_{mean}, SSH, P, es-ea, Rs, and W) performed the best as compared with all other models considered in this study. This strongly justifies the potential utility of the hybrid SVR-KHA model for estimating daily evaporation rates in coastal regions of Iran.

Compliance with ethical standards

Conflict of interest The authors declare that they have no conflict of interest.

References

Abualigah LM, Khader AT, Hanandeh ES, Gandomi AH (2017) A novel hybridization strategy for krill herd algorithm applied to clustering techniques. Appl Soft Comput 60:423–435

Aghelpour P, Mohammadi B, Biazar SM (2019) Long-term monthly average temperature forecasting in some climate types of Iran, using the models SARIMA, SVR, and SVR-FA. Theor Appl Climatol 138:1471–1480

Al-Shammari ET, Mohammadi K, Keivani A, Hamid SHA, Akib S, Shamshirband S, Petkovíc D (2016) Prediction of daily dewpoint temperature using a model combining the support vector machine with firefly algorithm. J Irrig Drain Engng 142:04016013. https://doi.org/10.1061/(ASCE)IR.1943-4774.0001015

Aybar-Ruiz A, Jiménez-Fernández S, Cornejo-Bueno L, Casanova-Mateo C, Sanz-Justo J, Salvador-González P, Salcedo-Sanz S (2016) A novel grouping genetic algorithm–extreme learning machine approach for global solar radiation prediction from numerical weather models inputs. Sol Energy 132:129–142

Dalkili Y, Okkan U, Baykan N (2014) Comparison of different ANN approaches in daily pan evaporation prediction. J Water Resour Prot 6(4):319–326

Deo RC, Samui P, Kim D (2016) Estimation of monthly evaporative loss using relevance vector machine, extreme learning machine and multivariate adaptive regression spline models. Stoch Env Res Risk Assess 30(6):1769–1784

Ding RS, Kang SZ, Li FS et al (2011) Evaluating eddy covariance method by largescale weighing lysimeter in a maize field of Northwest China. Agric Water Manag 98(1):87–95

Donohue RJ, Mcvicar TR, Roderick ML (2010) Assessing the ability of potential evaporation formulations to capture the dynamics in evaporative demand within a changing climate. J Hydrol 386(1):186–197

Estévez J, García-Marín AP, Morábito JA, Cavagnaro M (2016) Quality assurance procedures for validating meteorological input variables of reference evapotranspiration in Mendoza province (Argentina). Agric Water Manag 172(2016):96–109

Fan J, Wu L, Zhang F, Xiang Y, Zheng J (2016) Climate change effects on reference crop evapotranspiration across different climatic zones of China during 1956–2015. J Hydrol 542:923–937

Fan J, Chen B, Wu L, Zhang F, Lu X, Xiang Y (2018a) Evaluation and development of temperature-based empirical models for estimating daily global solar radiation in humid regions. Energy 144:903–914

Fan J, Wang X, Wu L, Zhang F, Bai H, Lu X, Xiang Y (2018b) New combined models for estimating daily global solar radiation based on sunshine duration in humid regions: a case study in South China. Energy Convers Manag 156:618–625

Feng S, Hu Q, Qian W (2004) Quality control of daily meteorological data in China, 1951–2000: a new dataset. Int J Climatol 24(7):853–870

Feng Y, Cui N, Gong D, Zhang Q, Zhao L (2017) Evaluation of random forests and generalized regression neural networks for daily reference evapotranspiration modelling. Agric Water Manag 193:163–173

Feng Y, Jia Y, Zhang Q, Gong D, Cui N (2018) National-scale assessment of pan evaporation models across different climatic zones of China. J Hydrol 564:314–328

Gandomi AH, Alavi AH (2012) Krill herd: a new bio-inspired optimization algorithm. Commun Nonlinear Sci Numer Simul 17(12):4831–4845

Ghorbani MA, Shamshirband S, Haghi DZ, Azani A, Bonakdari H, Ebtehaj I (2017) Application of firefly algorithm based support vector machines for prediction of field capacity and permanent wilting point. Soil Tillage Res 172:32–38

Ghorbani MA, Deo RC, Yaseen ZM, H. Kashani M, Mohammadi B (2018) Pan evaporation prediction using a hybrid multilayer perceptron-firefly algorithm (MLP-FFA) model: case study in North Iran. Theor Appl Climatol 133(3–4):1119–1131

Goyal MK, Bharti B, Quilty J, Adamowski J, Pandey A (2014) Modeling of daily pan evaporation in subtropical climates using ANN, LS-SVR, fuzzy logic, and ANFIS. Expert Syst Appl 41(11):5267–5276

Gundalia MJ, Dholakia MB (2013) Estimation of pan evaporation using mean air temperature and radiation for monsoon season in Junagadh region. Int J Eng Res Appl 3(6):64–70

Jahani B, Mohammadi B (2019) A comparison between the application of empirical and ANN methods for estimation of daily global solar radiation in Iran. Theor Appl Climatol 137(1–2):1257–1269

Kavousi-Fard A, Samet H, Marzbani F (2014) A new hybrid modified firefly algorithm and support vector regression model for accurate short term load forecasting. Expert Syst Appl 41(13):6047–6056

Khoob AR (2008) Artificial neural network estimation of reference evapotranspiration from pan evaporation in a semi-arid environment. Irrig Sci 27(1):35–39

Kim S, Kim HS (2008) Neural networks and genetic algorithm approach for nonlinear evaporation and evapotranspiration modeling. J Hydrol 351:299–317

Kim S, Shiri J, Kisi O (2012) Pan evaporation modeling using neural computing approach for different climatic zones. Water Resour Manag 26(11):3231–3249

Kim S, Shiri J, Kisi O, Singh VP (2013) Estimating daily pan evaporation using different data-driven methods and lag-time patterns. Water Resour Manag 27(7):2267–2286

Kim S, Lee YH, Kim KR, Park YS (2014) Analysis of surface energy balance closure over heterogeneous surfaces. Asia-Pac J Atmos Sci 50(1):553–565

Kim S, Shiri J, Singh VP, Kisi O, Landeras G (2015) Predicting daily pan evaporation by soft computing models with limited climatic data. Hydrol Sci J 60(6):1120–1136

Kisi O (2008) Daily pan evaporation modeling using multi-layer perceptrons and radial basis neural networks. Hydrol process. Hydrol Process 23(2):213–223

Kisi O (2013) Evolutionary neural networks for monthly pan evaporation modeling. J Hydrol 498(12):36–45

Kisi O (2015) Pan evaporation modeling using least square support vector machine, multivariate adaptive regression splines and M5 model tree. J Hydrol 528:312–320

Kisi O, Tombul M (2013) Modeling monthly pan evaporations using fuzzy genetic approach. J Hydrol 477(477):203–212

Lin GF, Lin HY, Wu MC (2013) Development of a support-vector-machine-based model for daily pan evaporation estimation. Hydrol Process 27(22):3115–3127

Liu W, Sun F (2016) Assessing estimates of evaporative demand in climate models using observed pan evaporation over China. J Geophys Res Atmos 121(14):8329–8349

Lu X, Ju Y, Wu L, Fan J, Zhang F, Li Z (2018) Daily pan evaporation modeling from local and cross-station data using three tree-based machine learning models. J Hydrol 566:668–684

Majhi B, Naidu D (2020) Pan evaporation modeling in different agroclimatic zones using functional link artificial neural network. Information Processing in Agriculture

Majhi B, Naidu D, Mishra AP, Satapathy SC (2019) Improved prediction of daily pan evaporation using deep-LSTM model. Neural Comput Appl:1–16

Malik A, Kumar A (2015) Pan evaporation simulation based on daily meteorological data using soft computing techniques and multiple linear regression. Water Resour Manag 29(6):1859–1872

Mehr AD, Nourani V, Khosrowshahi VK, Ghorbani MA (2019) A hybrid support vector regression–firefly model for monthly rainfall forecasting. Int J Environ Sci Technol 16(1):335–346

Moazenzadeh R, Mohammadi B (2019) Assessment of bio-inspired meta-heuristic optimization algorithms for estimating soil temperature. Geoderma 353:152–171

Moazenzadeh R, Mohammadi B, Shamshirband S, Chau KW (2018) Coupling a firefly algorithm with support vector regression to predict evaporation in northern Iran. Eng Appl Comput Fluid Mech 12(1):584–597

Mohammadi B (2019a) Letter to the editor "estimation of sodium adsorption ratio indicator using data mining methods: a case study in Urmia Lake basin, Iran" by Mohammad Taghi Sattari, Arya Farkhondeh, and John Patrick Abraham. Environ Sci Pollut Res 26(10):10439–10440

Mohammadi B (2019b) Predicting total phosphorus levels as indicators for shallow lake management. Ecol Indic 107:105664

Mohammadi B (2020) Letter to the editor "modeling daily suspended sediment load using improved support vector machine model and genetic algorithm". Environ Sci Pollut Res:1–2

Mohammadi B, Aghashariatmadari Z (2020) Estimation of solar radiation using neighboring stations through hybrid support vector regression boosted by krill herd algorithm. Arab J Geosci 13(10)

Mohammadi B, Mehdizadeh S (2020) Modeling daily reference evapotranspiration via a novel approach based on support vector regression coupled with whale optimization algorithm. Agric Water Manag 237:106145

Mohammadi B, Linh NTT, Pham QB, Ahmed AN, Vojteková J, Yiqing G, Abba SI, El-Shafie A (2020) Adaptive neuro-fuzzy inference system coupled with shuffled frog leaping algorithm for predicting river stream flow time series. Hydrol Sci J. https://doi.org/10.1080/02626667.2020.1758703

Pham QB, Afan HA, Mohammadi B et al (2020) Hybrid model to improve the river streamflow forecasting utilizing multi-layer perceptron-based intelligent water drop optimization algorithm. Soft Comput. https://doi.org/10.1007/s00500-020-05058-5

Piri J, Ansari H, Iran R (2012) Daily pan evaporation modelling with ANFIS and NNARX. Int J Agric Res 31(2):51–64

Piri J, Mohammadi K, Shamshirband S et al (2016) Assessing the suitability of hybridizing the cuckoo optimization algorithm with ANN and ANFIS techniques to predict daily evaporation. Environ Earth Sci 75(3):1–13

Prime E, Leung A, Tran D, Gill H, Solomon D, Qiao G, Dagley I (2012) New technology to reduce evaporation from large water storages. Waterlines Report Series No 80, June 2012

Roderick ML, Sun F, Lim WH, Farquha GD (2014) A general framework for understanding the response of the water cycle to global warming over land and ocean. Hydrol Earth Syst Sci 18:1575–1589

Sanikhani H, Kisi O, Nikpour MR, Dinpashoh Y (2012) Estimation of daily pan evaporation using two different adaptive neuro-fuzzy computing techniques. Water Resour Manag 26(15):4347–4365

Schwarz G (1978) Estimating the dimension of a model. Ann Stat 6(2):461–464

Shiri J, Marti P, Singh VP (2014) Evaluation of gene expression programming approaches for estimating daily evaporation through spatial and temporal data scanning. Hydrol Process 28(3):1215–1225

Singh VP, Xu C (2015) Evaluation and generalization of 13 equations for determining free water evaporation. Hydrol Process 11(3):311–323

Tabari H, Marofi S, Sabziparvar AA (2009) Estimation of daily pan evaporation using artificial nueral network and multivariate nonlinear regression. Irrig Sci 28(5):399–406

Vaheddoost B, Guan Y, Mohammadi B (2020) Application of hybrid ANN-whale optimization model in evaluation of the field capacity and the permanent wilting point of the soils. Environ Sci Pollut Res:1–11

Vapnik VN, Chervonenkis AJ (1974) Theory of pattern recognition. Nauka, Moscow

Vapnik V, Golowich SE, Smola AJ (1997) Support vector method for function approximation, regression estimation and signal processing. In: Advances in neural information processing systems, pp 281–287

Vicente-Serrano SM, Bidegain M, Tomas-Burguera M, Dominguez-Castro F, el Kenawy A, McVicar TR, Azorin-Molina C, López-Moreno JI, Nieto R, Gimeno L, Giménez A (2018) A comparison of temporal variability of observed and model-based pan evaporation over Uruguay (1973–2014). Int J Climatol 38(1):337–350

Wang L, Kisi O, Zounemat-Kermani M et al (2016a) Pan evaporation modeling using six different heuristic computing methods in different climates of China. J Hydrol 544

Wang Y, Feng D, Li D et al (2016b) A mobile recommendation system based on logistic regression and gradient boosting decision trees. In: International joint conference on neural networks. IEEE, pp 1896–1902

Wang L, Kisi O, Hu B et al (2017a) Evaporation modelling using different machine learning techniques. Int J Climatol 37(S1):1076–1092

Wang L, Niu Z, Kisi O, Li C, Yu D (2017b) Pan evaporation modeling using four different heuristic approaches. Comput Electron Agric 140:203–213

Wang L, Kisi O, Zounemat-Kermani M, Li H (2017c) Pan evaporation modeling using six different heuristic computing methods in different climates of China. J Hydrol 544:407–427

Wang H, Yan H, Zeng W, Lei G, Ao C, Zha Y (2020) A novel nonlinear Arps decline model with salp swarm algorithm for predicting pan evaporation in the arid and semi-arid regions of China. J Hydrol 124545

Wu L, Huang G, Fan J, Ma X, Zhou H, Zeng W (2020) Hybrid extreme learning machine with meta-heuristic algorithms for monthly pan evaporation prediction. Comput Electron Agric 168:105115

Xu C, Singh VP (1998) Dependence of evaporation on meteorological variables at different time-scales and inter comparison of estimation methods. Hydrol Process 12:429–442

Xu C, Singh VP (2000) Evaluation and generalization of radiation-based methods for calculating evaporation. Hydrol Process 14:339–349

Xu C, Singh VP (2001) Evaluation and generalization of temperature-based methods for calculating evaporation. Hydrol Process 15:305–319

Yang HB, Yang DW (2012) Climatic factors influencing changing pan evaporation across China from 1961 to 2001. J Hydrol 414–415:184–193

Terms and Conditions

Springer Nature journal content, brought to you courtesy of Springer Nature Customer Service Center GmbH (“Springer Nature”).
Springer Nature supports a reasonable amount of sharing of research papers by authors, subscribers and authorised users (“Users”), for small-scale personal, non-commercial use provided that all copyright, trade and service marks and other proprietary notices are maintained. By accessing, sharing, receiving or otherwise using the Springer Nature journal content you agree to these terms of use (“Terms”). For these purposes, Springer Nature considers academic use (by researchers and students) to be non-commercial.
These Terms are supplementary and will apply in addition to any applicable website terms and conditions, a relevant site licence or a personal subscription. These Terms will prevail over any conflict or ambiguity with regards to the relevant terms, a site licence or a personal subscription (to the extent of the conflict or ambiguity only). For Creative Commons-licensed articles, the terms of the Creative Commons license used will apply.
We collect and use personal data to provide access to the Springer Nature journal content. We may also use these personal data internally within ResearchGate and Springer Nature and as agreed share it, in an anonymised way, for purposes of tracking, analysis and reporting. We will not otherwise disclose your personal data outside the ResearchGate or the Springer Nature group of companies unless we have your permission as detailed in the Privacy Policy.
While Users may use the Springer Nature journal content for small scale, personal non-commercial use, it is important to note that Users may not:

1. use such content for the purpose of providing other users with access on a regular or large scale basis or as a means to circumvent access control;
2. use such content where to do so would be considered a criminal or statutory offence in any jurisdiction, or gives rise to civil liability, or is otherwise unlawful;
3. falsely or misleadingly imply or suggest endorsement, approval , sponsorship, or association unless explicitly agreed to by Springer Nature in writing;
4. use bots or other automated methods to access the content or redirect messages
5. override any security feature or exclusionary protocol; or
6. share the content in order to create substitute for Springer Nature products or services or a systematic database of Springer Nature journal content.

In line with the restriction against commercial use, Springer Nature does not permit the creation of a product or service that creates revenue, royalties, rent or income from our content or its inclusion as part of a paid for service or for other commercial gain. Springer Nature journal content cannot be used for inter-library loans and librarians may not upload Springer Nature journal content on a large scale into their, or any other, institutional repository.
These terms of use are reviewed regularly and may be amended at any time. Springer Nature is not obligated to publish any information or content on this website and may remove it or features or functionality at our sole discretion, at any time with or without notice. Springer Nature may revoke this licence to you at any time and remove access to any copies of the Springer Nature journal content which have been saved.
To the fullest extent permitted by law, Springer Nature makes no warranties, representations or guarantees to Users, either express or implied with respect to the Springer nature journal content and all parties disclaim and waive any implied warranties or warranties imposed by law, including merchantability or fitness for any particular purpose.
Please note that these rights do not automatically extend to content, data or other material published by Springer Nature that may be licensed from third parties.
If you would like to use or distribute our Springer Nature journal content to a wider audience or on a regular basis or in any other manner not expressly permitted by these Terms, please contact Springer Nature at

onlineservice@springernature.com